LINEAR IMPEDANCE STUDIES OF VOLTAGE-DEPENDENT CONDUCTANCES IN TISSUE CULTURED CHICK HEART CELLS

LISA EBIHARA AND RICHARD T. MATHIAS
Department of Physiology, Rush Medical College, Chicago, Illinois 60612

ABSTRACT Plateau and pacemaker currents from tissue cultured clusters of embryonic chick heart cells were studied in the time domain, using voltage-clamp steps, and in the frequency domain, using a wide-band noise input superimposed on a steady holding voltage. In the presence of tetrodotoxin to block the sodium channel, a depolarizing voltage step into the plateau range elicited: (*a*) a rapid (≈2 ms) activation of the slow inward current; (*b*) a subsequent slower (≈25 ms) decline in the slow inward current; and (*c*) activation of a very slow (5 to 10 s) outward current. Impedance studies in this voltage range could clearly resolve two voltage-dependent processes, which appeared to correspond to points *b* and *c* above because of their voltage dependence, pharmacology, and time constants. A correlate of point *a* was also probably present but difficult to resolve owing to the fast time constant of activation for the slow inward channel. At voltages negative to −50 mV a new voltage-dependent process could be resolved, which, because of its voltage dependence and time constant, appeared to represent the pacemaker channel (also termed I_f or I_{K2}). In the Appendix, linear models of voltage-dependent channels and ion accumulation/depletion are derived and these are compared with our data. Most of the above-mentioned processes could be attributed to voltage-dependent channels with kinetics similar to those observed in time domain, voltage-clamp studies. However, the frequency domain correlate of the decline of the slow inward current was incompatible with channel gating, rather, it appears accumulation/depletion of calcium may dominate the decline in this preparation.

INTRODUCTION

The membrane channels underlying generation of the cardiac action potential have been a subject of interest for many years. The earliest models, which dated back to the pre–voltage-clamp era, were simple modifications of the original Hodgkin-Huxley (H-H) equations (Fitzhugh, 1960). In later years, following application of the voltage-clamp technique to cardiac muscle, it became apparent that there were small, slowly changing currents in cardiac muscle, which could not be adequately described by simple modifications of the H-H equations (Attwell et al., 1979; Levis et al., 1983). Unfortunately, interpretation of currents measured in voltage clamp proved to be difficult because of: (*a*) accumulation/depletion of ions in the narrow clefts between closely packed cells; (*b*) spatial and temporal nonuniformity of transmembrane potential; (*c*) superposition of currents due to different channel populations. To simplify the interpretation of currents, a number of investigators have turned to voltage-clamping preparations with simpler geometries, such as single heart cells (Hume and Giles, 1983; Lee et al., 1979; Brown et al., 1981; Bodewei et al., 1982; Cachelin et al., 1983), or tissue cultured preparations (Ebihara et al., 1980).

Another approach to characterizing the currents underlying the action potential is small signal impedance analysis (Fishman et al., 1979 and 1981; Clapham and DeFelice, 1982; Mathias et al., 1981*b*). The main advantages of applying this technique to cardiac muscle are: (*a*) it allows channel properties and structural properties to be analyzed simultaneously; (*b*) it does not require rapid, spatially uniform control of transmembrane voltage, rather the only requirement is that the zero frequency (DC) transmembrane potential be spatially uniform; and (*c*) the interaction of membrane channels, membrane capacitance, and series resistance can be quantitatively analyzed. Furthermore, small signal impedance analysis may be helpful in distinguishing between different physical processes that are capable of yielding similar macroscopic behavior in the time domain. The object of the present study is to measure the linear impedance of spherical clusters of chick embryonic heart cells at different holding potentials, and from these data to extract information on the mechanisms underlying the nonlinear, time and voltage-dependent currents.

METHODS

Tissue Culture

The tissue cultured clusters were prepared from the hearts of 11-d chick embryos (atrial and ventricular tissue) using the techniques described in Ebihara et al., 1980. The culture medium was free of antibiotics and contained 55% medium 199 (GIBCO, Grand Island, NJ), 41% K-free

Dr. L. Ebihara's present address is the Department of Physiology, University of Colorado, Denver, Colorado.

Earle's balanced salt solution, 2% fetal calf serum (Granite Diagnostics, Burlington, NC), and 2% chick embryo extract (Kaighn et al., 1966). The concentrations of Na^+, K^+, and Ca^{++} for this medium were measured and reported in Ebihara et al. (1980) as: Na = 145 mM; K = 3.5 mM; Ca^{++} = 4.1 mM.

Electrophysiology

The culture medium was covered by a thin layer of mineral oil (Sigma Chemical Corp., St. Louis, MO) to prevent evaporation. A gassing ring was positioned around the dish to provide a mixture of 5% O_2/95% air in order to control pH at ~7.4. All experiments were performed at room temperature (22°C). Intracellular microelectrodes (20–40 MΩ) were filled with 3 M KCl and positioned around the culture dish using two hydraulic micromanipulators (MO-102; Narishige Scientific Laboratory, Tokyo, Japan), which were mounted on Leitz micromanipulators (E. Leitz Inc., Rockleigh, NJ). Both electrodes were painted to within 200 μm of their tips with conductive silver paint (High Purity Silver Paint, SPI Supplies Div. of Structure Probe Inc., Westchester, PA) and then insulated with varnish (Red GLPT Insulating Varnish, GC Electronics Div. of Hydrometals, Inc., Rockford, IL; Humiseal, Humiseal Division, Columbia Chase Corporation, Woodside, NY). The current measuring circuit and the potential and current recording circuits are described in Mathias et al. (1981*a*).

The preparation was first impaled with two microelectrodes, one for passing current and one for recording voltage. Only those preparations that could be penetrated by a second microelectrode without a fall in resting potential of more than 2 to 3 mV were used. The cells were generally spontaneously active (except in the presence of both TTX and D600) so we had to either pass a DC current or apply the voltage clamp to stop them from beating. A small white noise signal (~3 mV peak-to-peak) was superimposed on the holding potential and the perturbations to intracellular voltage and total bath current were recorded. The impedance at each holding potential was determined in accordance with the procedures in Mathias et al., (1981*a*). The impedance is the ratio of preparation voltage to preparation current and so it does not, in principle, depend on the external circuitry that drives the system in either the voltage clamp mode or current clamp mode.

Linearity of the impedance was tested as in Mathias et al. (1981*b*, Fig. 5) and by recording the coherence function, which is defined in Mathias et al. (1979). In the voltage-clamp mode of recording the impedance, the coherence was generally low at the resonant peak, however, the coherence measures both signal-to-noise and linearity with no distinction. In voltage clamp, the current at the resonant peak is minimum and therefore the signal-to-noise is minimum. The same experiment in the current-clamp mode produces the best signal-to-noise ratio at the peak of the resonance and indeed the coherence was best in this frequency range. Thus, we found no evidence that our results are contaminated by nonlinear effects.

Pharmacological Agents

Tetrodotoxin (Calbiochem Corp., LaJolla, CA) and compound D600-methoxyverapamil (hereafter referred to as D600) (a gift from Knoll AG, Ludwigshafen am Rhein, Federal Republic of Germany) were dissolved in distilled water to make up stock solutions of 400 μg/ml and 100 μg/ml, respectively, and administered via a lambda micropipette under mineral oil directly into the culture medium at the edge of the culture dish. It usually required ~5 min for the agent to have its maximum measureable effect on the membrane channels. If complete equilibration occurred, the final concentrations of each compound in the culture dish were 100 and 2.4 μM, respectively. Nifedipine (Pfizer, New York) was added from an ethanolic stock solution after 50× dilution in distilled water to give a final concentration of 0.3 μM. The nifedepine containing solution was kept in the dark as much as was possible.

THEORY

The equivalent circuit for a cluster is based on the model of Eisenberg et al. (1979) for current flow in spherical syncytia. This model has been applied previously to heart cell clusters by Mathias et al. (1981*b*). The membranes of cells comprising a cluster are assumed to be homogeneous. We have modeled the specific admittance per unit area of membrane as

$$Y_m(j\omega) = G_m + j\omega C_m + \sum_{k=1}^{N} \frac{G_k}{1 + j\omega/\omega_k}. \tag{1}$$

The parameter C_m (F/cm²) represents the passive, voltage-independent membrane capacitance: G_m (S/cm²) is the frequency-independent component of membrane conductance at the DC membrane voltage to which the cluster has been clamped; the G_ks (S/cm²) and ω_ks (s^{-1}) are included to model the linear response of time-dependent processes that manifest themselves at a given steady-state voltage and are driven by small voltage or current perturbations about the DC level. The physical interpretation of these parameters is derived in the Appendix.

The spherical syncytium model of Eisenberg et al. (1979) predicts the linear response of a cluster can be described by

$$Z(j\omega) = \frac{1}{4\pi a^2[Y_m(j\omega) + Y_e(j\omega)]} + R_S, \tag{2}$$

where R_S (Ω) is the lumped series resistance, due in large measure to the point source effect discussed in Mathias et al. (1981) but also including the bath, bath electrode, and any other structures in series with the outer surface. Most of the membrane within a cluster faces small intercellular clefts, which provide a distributed resistance in series with these inner membranes. The parameter $Y_e(j\omega)$ (S/cm²) represents the input admittance (per unit area of outer spherical surface) of the cablelike structure of small intercellular clefts lined with membranes that are described by Y_m in Eq. 1. These clefts extend from the surface to the center of the cluster. Y_e is defined by

$$Y_e(j\omega) = \frac{\gamma}{R_e}\left(\coth \gamma a - \frac{1}{\gamma a}\right), \tag{3}$$

where

$$\gamma^2 = R_e \frac{S_m}{V_T} Y_m(j\omega), \tag{4}$$

R_e (Ωcm) is the effective resistivity of the intercellular volume within the cluster and S_m/V_T (cm⁻¹) is the average amount of membrane per unit volume of tissue, and a is the cluster radius.

When the value of γa is small, Eq. 3 for Y_e can be approximated by

$$Y_e(j\omega) \longrightarrow \frac{a}{3}\frac{S_m}{V_T} Y_m(j\omega). \qquad \gamma a \longrightarrow 0 \tag{5}$$

This result is most likely to be valid at low frequency or DC since the value of γ increases as the square root of frequency. When Eq. 5 is indeed valid, the clusters will have essentially a uniform voltage across all of their membranes. From Tables I to III in the Results section, we see the DC membrane conductance, G_m, is typically 50×10^{-6} S/cm². This value of G_m, in connection with the other relevant parameters presented in Table I, gives a DC value of $\gamma a = 0.48$. The fractional change in extracellular voltage relative to the induced intracellular voltage is maximal at the center of the cluster and is given by $1 - \gamma a/\sinh \gamma a$ (Eisenberg et al., 1979). Thus, the induced extracellular DC voltage at the center of a cluster is typically 3.7% of the change in intracellular voltage. Hence we will assume the DC transmembrane voltage is the same throughout the cluster, consequently the average conductance G_m as well as the values of the G_ks and ω_ks are assumed to be uniform throughout the cluster. The model of Eisenberg et al. (1979) assumes the specific membrane properties do not vary radially, so if the DC transmembrane voltage is not uniform, this model is a poor or invalid representation of the tissue.

RESULTS

Voltage-Clamp Experiments

In spherical clusters of chick embryonic heart cells there are two time-dependent inward currents, I_{Na}, I_{si}, one time-dependent outward current, I_X, and the pacemaker current, I_f, which can be distinguished on the basis of differences in activation voltages, rate constants, and pharmacology (Josephson and Sperelakis, 1982; Clay and Shrier, 1981*a*, 1981*b*; Ebihara et al., 1980; Nathan and DeHaan, 1979).

Fig. 1 shows the slow inward current elicited in response to depolarizing voltage-clamp steps at 22°C. TTX (100 μM) was added to block the fast inward current. The slow inward current first became noticeable at an intracellular voltage of around −40 mV. The current reached a peak in 1–2 ms, then declined to its final value in under 50 ms. The time-to-peak of the slow inward current in this preparation is much more rapid than that reported for other syncytial preparations (reviewed by Reuter, 1979).

The slow inward current was followed by a slow transient outward current, I_X, illustrated in Fig. 2. The delayed outward current had a threshold around −40 mV and reached a steady state in 3–10 s. Following repolarization, a decaying outward tail current was observed. Both the slow inward current and the delayed outward current disappeared following application of D600, suggesting the slow outward current might be a Ca-activated K channel, similar to the channel that has now been observed in many different preparations (Meech, 1978; Lux et al., 1981, Marty, 1981) or it might be a D600 blockable K channel (Kass, 1984).

The time and voltage dependence of the pacemaker current, I_f, were not explored in these voltage-clamp studies, however, Clay and Shrier (1981*a*) reported the presence of a time-dependent current that is carried by potassium ions in clusters prepared from ventricles of 7-d chick embryos.

Impedance Analysis

The impedance studies were performed by voltage clamping the preparation to a selected holding potential onto which a small wide-band stochastic noise signal was superimposed. Fig. 3 *A* shows the impedance of a cluster at −42 and −45 mV. The solid lines represent the best fit of the theoretical model to the data. At −45 mV no resonant peak is observed and the membrane can be described by the simple resistor-capacitor circuit given by Eq. 1 with the G_ks = 0. When the preparation is depolarized from −45 to −42 mV, a large resonant peak appears and a more complicated circuit, which includes G_1, ω_1, G_2, and ω_2, is required to describe the membrane impedance. In this preparation, the impedance changes reversed when we repolarized the membrane back to −45 mV. However, in other preparations, when several potential changes were

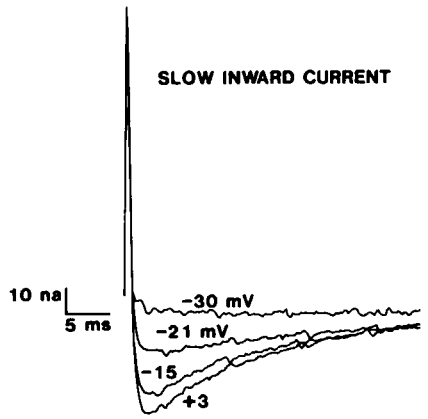

FIGURE 1 Current traces recorded during a series of depolarizing voltage-clamp steps. Holding potential, −40 mV.

studied and the experiments required more time, there were usually small changes in the impedance.

Fig. 3 *B* shows the same data as in Fig. 3 *A* with the two curves superimposed in order to better illustrate the dramatic change in the impedance as a function of potential. For clarity, only the theoretical fits to the data are shown. At potentials more positive than −30 mV the amplitude of the resonant peak decreases and the zero phase crossing shifts to higher frequencies as illustrated in Fig. 4. The frequency at which the phase angle equals zero is called the resonance frequency, f_0. The significance of f_0 is that it is the frequency at which the preparation will tend to oscillate.

The data were analyzed by first estimating the passive membrane parameters, either by measuring the impedance at a hyperpolarized voltage where the G_ks of Eq. 1 are zero, or by determining which values of passive parameters best described the data at all potentials. The average radius and values for C_m, R_s, and R_e derived from a number of different impedance data sets are given in Table I. The

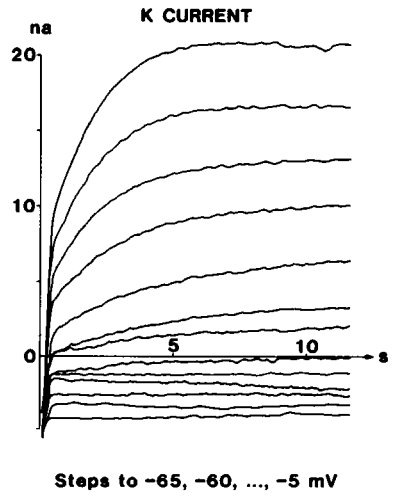

FIGURE 2 Delayed outward current elicited by depolarization from a holding potential of −75 mV in steps of 5 mV.

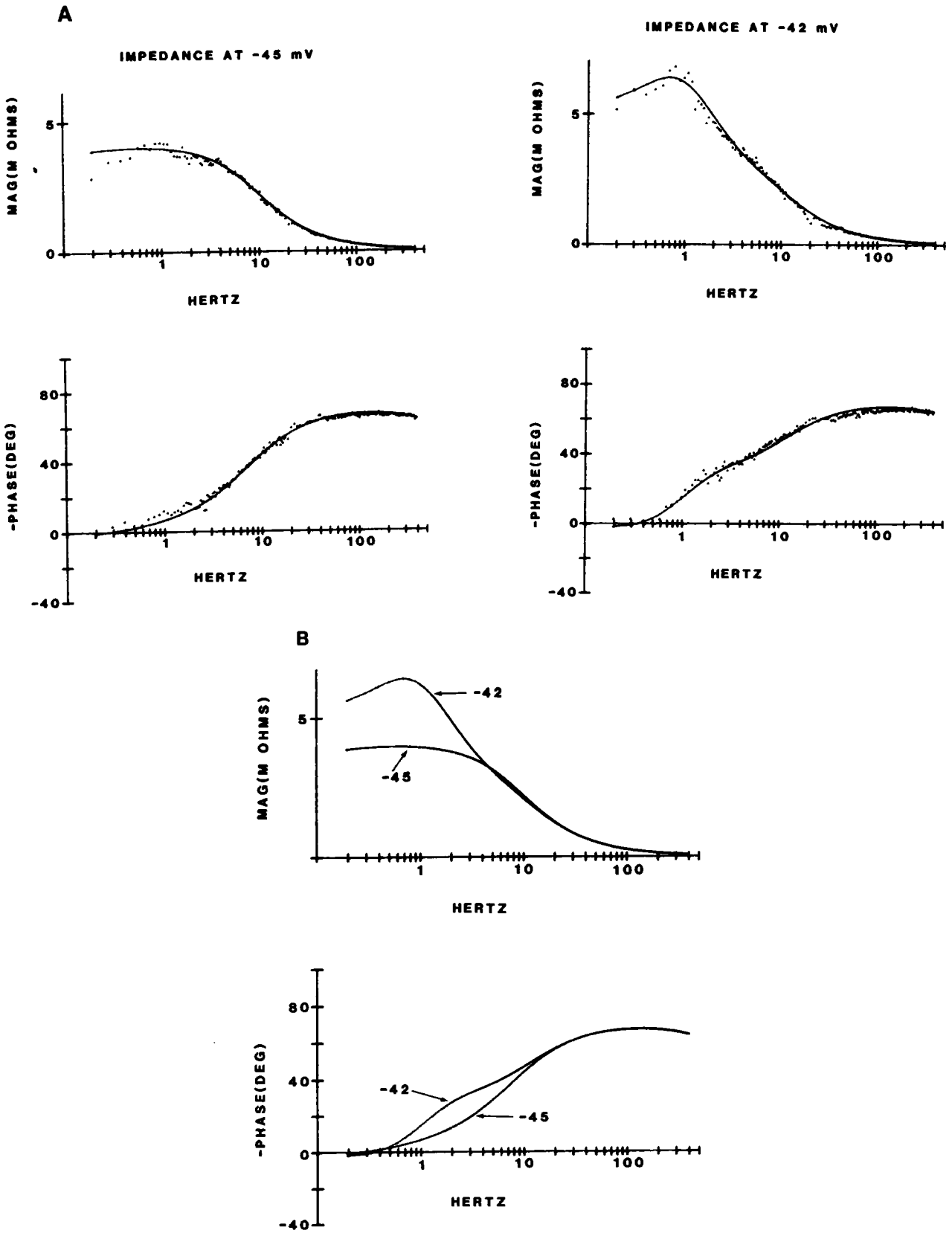

FIGURE 3 Plots of the magnitude and phase of the impedance of chick embryonic heart cell clusters at two different holding potentials. The solid line is the theoretical curve determined by the best fit of the theory. (*B*) Plots of the theoretical fits shown in *A* superimposed.

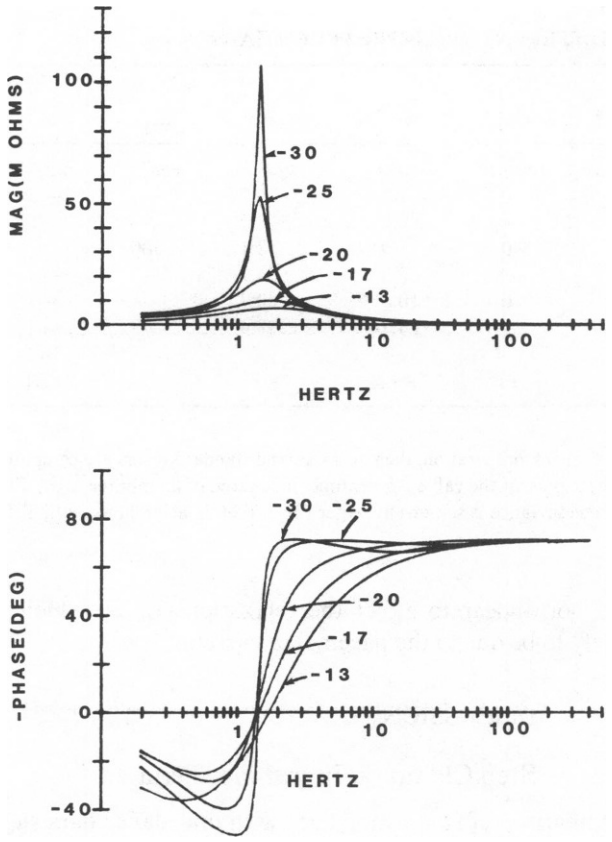

FIGURE 4 Plots of the fits of the theory to the magnitude and phase of the heart clusters at five different holding potentials. The data in this experiment were obtained in the current clamp mode.

value for S_m/V_T was taken from earlier morphological measurements (Mathias et al., 1981*b*). The curve fitting to obtain G_ks and ω_ks was done using C_m, R_s, and R_e as fixed parameters in the model, based on their values determined at voltages where the G_ks were nearly zero.

Two relaxation elements were needed to fit the data in most of the experiments performed at steady potentials above −40 mV: a negative conductance G_2 with a relaxation time of 10–50 ms and a positive conductance G_1 with a relaxation time of 0.3–2 s. Both conductance terms increased concomitantly around −40 mV. Both conductances were blocked by D600 and nifedipine (see the section Drug Effects).

TABLE I
PASSIVE MEMBRANE PROPERTIES AND STRUCTURAL PROPERTIES

N	Radius	C_m	R_e	R_s
	μm	$\mu F/cm^2$	$K\Omega cm$	$K\Omega$
12	62	0.66	14.7	46.8
—	±2	±0.04	±5.0	±21.0

The mean values ±SEM are presented. We assume (S_m/V_T) = 8,000 cm^{-1} (Mathias et al., 1981). The typical membrane area in a cluster is given by $(4/3)\,\pi\,a^3\,(S_m/V_T)$ = 0.008 cm^2.

In addition, two of the clusters required a third relaxation (G_3, ω_3) in order to fit the data in the −40 to −10 mV range of voltage. The value of G_3 was negative and $(\omega_3/2\pi) \simeq 50$ Hz. The same term could be included for all of the other clusters as well, but the value of $\omega_3/2\pi \geq 50$ Hz was sufficiently high that simply adjusting G_m produced an indistinguishable fit to the data. The fast time constant and negative value of G_3 suggest the activation gate of the slow inward channel may be influencing our data but at most voltages and in most experiments it is too fast to be resolved as a separate component. Table II therefore combines the effect of G_3 into G_m.

The time constant, voltage dependence, and pharmacology of G_2 suggest we are recording the inactivation process for the slow inward current (see Fig. 2). If so, the negative sign of G_2 implies inactivation is dominated by accumulation/depletion of calcium, as described in the Appendix. The time constant, voltage dependence, and positive sign of G_1 suggest it represents the activation gate for the outward current shown in Fig. 2.

Fig. 5 shows the magnitude and phase of an aggregate at −50 and −55 mV. When the membrane potential was voltage clamped to −50 mV the membrane behaved like a simple resistor-capacitor circuit. At more hyperpolarized potentials a new resonance appeared, which could be distinguished from the relaxation G_1 in that it occurred (*a*) at a higher frequency and (*b*) in a different voltage range. Table II summarizes the results of three experiments performed at −50 and −55 mV. In a fourth experiment no resonant peak was observed over the potential range between −50 and −75 mV. G_4 has the correct voltage dependence and natural frequency to be the pacemaker current (Clay and Shrier, 1981*a*, *b*; DiFrancesco, 1981). The positive sign of G_4 is consistent with either an outward current, which activates on depolarization, or an inward current, which inactivates on depolarization.

Within the voltage ranges specified in Table II, there were further systematic changes in parameter values. However, the impedance studies required several minutes at each holding voltage and when we returned to a previous voltage, there were usually small changes in the impedance. Furthermore, curve fitting of the data showed we could obtain very similar fits when some fraction of G_1, G_2, or G_m was traded. Such trade-offs are within the variance of average values, so we do not consider the small systematic changes to be reliably recorded. We have therefore chosen to report average values within a voltage range.

Drug Effects

The effects of several cardioactive compounds such as D600, TTX, and nifedipine were tested in an attempt to separate the contributions of different time and voltage-dependent ionic channels. TTX caused no significant changes in impedance. The effect of D600 was to virtually

TABLE II
COMPARISON OF TISSUE PROPERTIES AT DIFFERENT HOLDING POTENTIALS

Voltage	N	Mean voltage	G_m*	G_1*	G_2*	G_3*	G_4*	ω_1	ω_2	ω_3	ω_4
mV		*mV*	*μS/μF*	*μS/μF*	*μS/μF*	*μS/μF*	*ms/μF*	*rad/s*	*rad/s*	*rad/s*	*rad/s*
$V_m \geq -20$	4	−11	79	128	−9	0	0	1.4	79.7	—	—
		±3	±20	±41	±6	—	—	±0.2	±18.2	—	—
$-20 > V_m \geq -40$	9	−36	38	25	−26	?	0	1.9	58.1	>300	—
		±2	±6	±5	±3	—	—	±0.3	±24.7	—	—
$-40 > V_m \geq -50$	9	−47	31	6	−5	0	0	10.3	80.7	—	—
		±1	±5	±1	±1	—	—	±4.7	±38.4	—	—
$-50 > V_m \geq -60$	3	−55	20	0	0	0	14	—	—	—	16.5
		+0	±3	—	—	—	±1	—	—	—	±7.1

The mean values and ± SEM are presented.
*These parameters are normalized by the specific membrane capacitance derived for each preparation, then averages and standard errors are computed. If the membrane capacitance is 1 $\mu F/cm^2$, then the reported values of conductance represent the value per centimeter squared of membrane area; if the morphologically determined value of membrane area is correct, then the specific conductance is somewhat larger (by 1/0.66 in accordance with Table I).

eliminate the resonant peak otherwise present at potentials positive to −40 mV as illustrated in Fig. 6. The model parameters used in fitting the data in Fig. 6 are given in Table III. In all of these experiments the data were well described by a model in which the G_ks were nearly all equal to zero. Application of 0.5–2.5 μM nifedipine also caused a reduction in both G_1 and G_2. However, this blockade was never as complete as that observed with D600. Nifedipine did not appear to affect the relaxation G_4, ω_4, which is likely to be due to the pacemaker current.

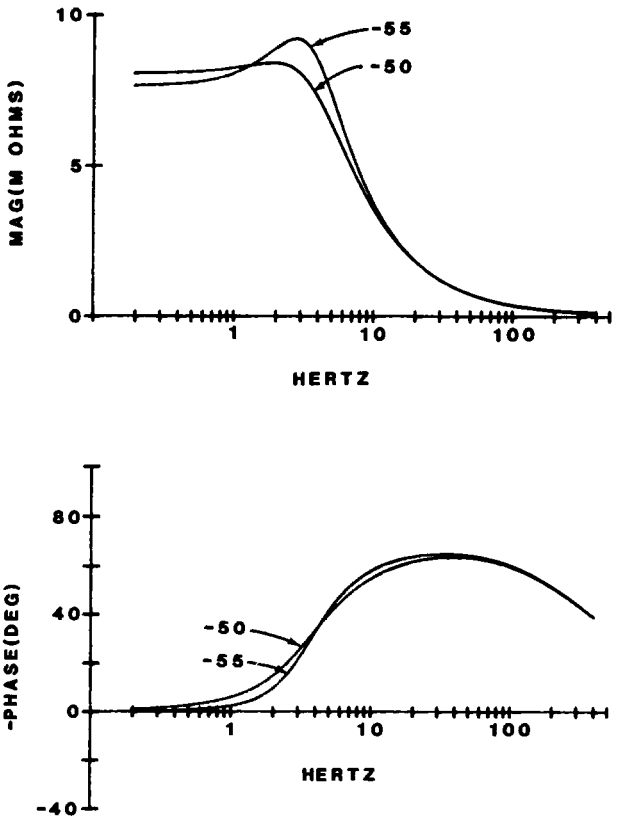

FIGURE 5 Plots of the fits of theory to the phase and magnitude of the impedance of the heart clusters at two hyperpolarized potentials.

DISCUSSION

Step Clamp vs. Impedance Data

Comparison of step-clamp data with impedance data suggests that the resonant peak observed at potentials positive to −40 mV is due to interaction of the slow inward current and the delayed outward current with the membrane capacitance. Both the slow inward current and the resonant peak have similar thresholds of activation and are blocked by the drug D600 but not TTX. The decrease in the resonant peak with depolarization parallels steady state activation of the delayed outward current. The two relaxation conductances in the impedance model have time constants that are similar to the time constants of activation and of the delayed outward current and decline of the slow inward current in the time domain. However, as derived in the Appendix, the sign of the negative conductance term is wrong for an inactivation gate being responsible for the decline of the slow inward current.

One explanation for our findings is that the decline of the slow inward current, observed under maintained depolarization, results from a drop in the calcium equilibrium potential produced by either depletion of calcium from a restricted extracellular space or accumulation of calcium intracellularly. Such a mechanism of inactivation has been suggested to occur in other excitable cells including skeletal muscle fibers (Almers and Palade, 1981; Almers et al., 1981) and inactivation of the slow inward current in sheep Purkinje strands (Levis et al., 1983).

It is clear that accumulation/depletion must occur whenever transmembrane currents are activated. However, the work of Reuter et al. (1982), Lee and Tsien (1982), Isenberg and Klöckner (1982), or Matteson and Armstrong (1984) show that calcium channels in heart

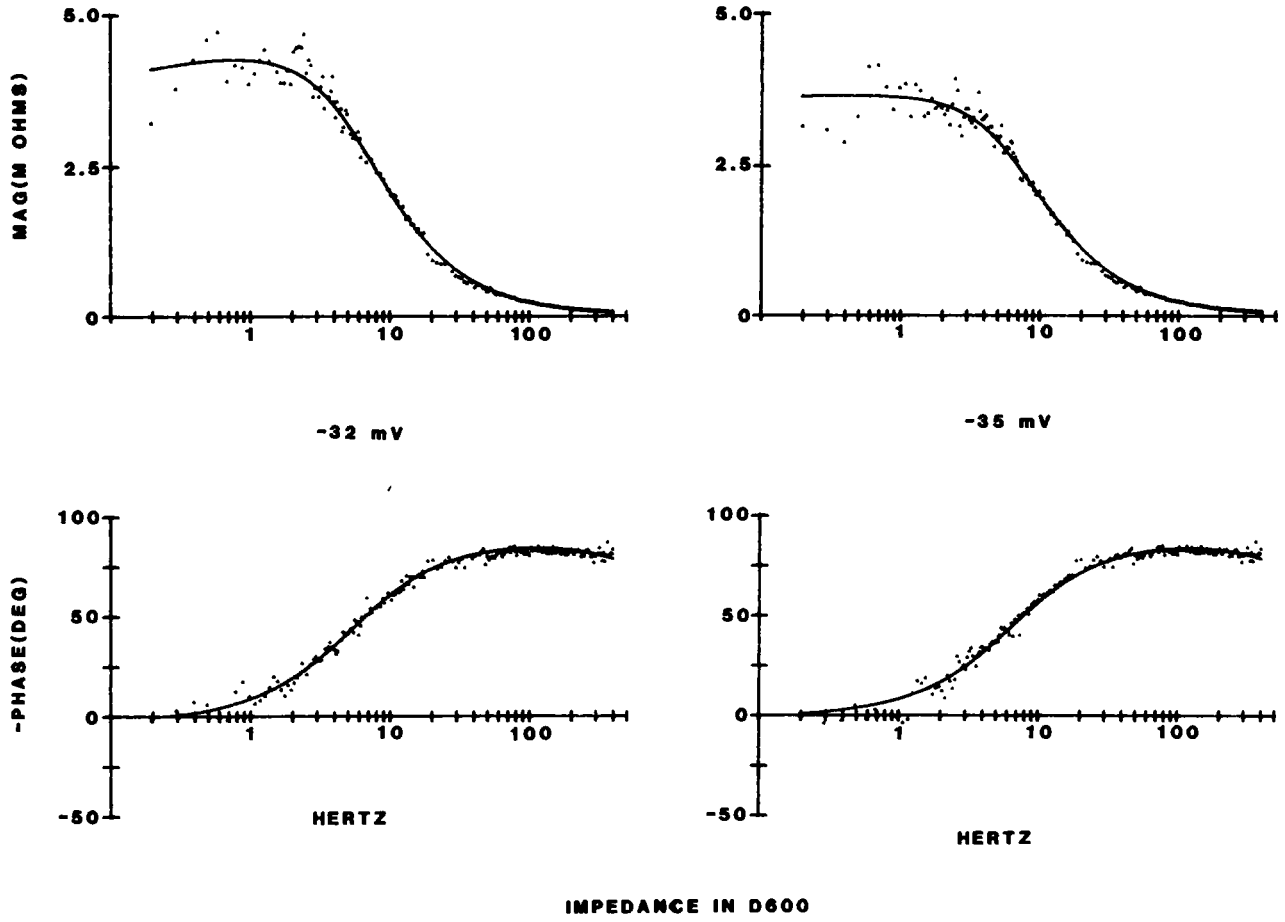

FIGURE 6 Plots of the magnitude and phase of the impedance of a heart cluster following application of D600. The solid line is the theoretical curve determined by the best fit of the theory. In this voltage range, a large resonance was always observed in the impedance in the absence of D600.

and other tissues have true gated inactivation. The relevant question for any tissue therefore seems to be: Does accumulation/depletion or gated inactivation occur first? In this tissue our impedance results suggest that accumulation/depletion is the more rapid process. Moreover, the time course of the decline of the slow inward current illustrated in Fig. 1 is significantly faster than that of gated inactivation as reported in the above references. Nevertheless, we believe gated inactivation must also be occurring.

TABLE III
MEMBRANE PARAMETER VALUES IN D600

N	Membrane voltage	G_m*	G_1*	G_2*	ω_1	ω_2
		$\mu S/\mu F$	$\mu S/\mu F$	$\mu S/\mu F$	*rad/s*	*rad/s*
1	−37	40	2	0	0.5	—
—	−35	33	4	0	1.2	—
—	−32	39	0	0	—	—
—	−30	31	0	0	—	—
—	−28	26	0	0	—	—

*These parameters are normalized by the specific membrane capacitance, C_m.

For example, from Table I we see that G_2 is maximal in the voltage range of $-40 \leq V_m \leq -20$ mV and it declines at voltages positive to -20 mV. We would not expect a significant decline in accumulation/depletion over this all voltage range, unless there is also a true gated inactivation that is causing $\bar{g}_{si}$ to go to zero. Presumably, because accumulation/depletion is dominating, we cannot resolve the frequency domain correlate of the gated inactivation.

The results in the Appendix allow us to quantitatively estimate whether or not accumulation/depletion can be sufficiently rapid to account for our observations. From Eqs. A15 and A20, one can see that the time constant for accumulation/depletion is directly proportional to the Ca concentration (the lower the calcium the faster the time constant) and inversely proportional to the surface-to-volume ratio of the compartment (the larger the surface-to-volume ratio the faster the time constant)

$$\tau_{i,c} \propto \overline{Ca}_{i,c}/(\bar{g}_{si}\, S_m/V_{i,c}),$$

where $\overline{Ca}_{i,c}$ is the average calcium concentration in the compartment of interest, $S_m/V_{i,c}$ is the surface of membrane per unit volume of the compartment, and $\bar{g}_{si}$ is the average membrane conductance for calcium. The intercel-

lular cleft volume is relatively small and consequently the surface of membrane per unit volume of cleft, S_m/V_c, is relatively large. However, the average calcium concentration is a few millimoles per liter in the clefts whereas the concentration within the cells is <1 μM. Thus, either τ_i or τ_c might be rapid: τ_c because of the large value of S_m/V_c and τ_i because of the small value of $\overline{Ca}_i$.

For the extracellular clefts, we can estimate the surface volume ratio by first estimating the volume fraction V_c/V_T from our measurement of the effective resistivity, R_e. Mathias (1983) shows that

$$R_e = \frac{\rho_e}{\tau V_c/V_T},$$

where ρ_e is the resistivity of bulk solution (about 50 Ωcm) and τ is the tortuosity factor ($\sim 2/3$ for a cluster). From Table I, we can estimate $V_c/V_T = 0.005$.

The effective diffusion coefficient for the clefts, D_c, can also be determined from R_e by the relationship

$$\frac{1}{R_e} = D_c \frac{F^2 c_0}{RT},$$

where c_0 is the concentration of ions in bulk solution ($\sim$300 mM). Thus, $D_c \simeq 5 \times 10^{-8}$ cm^2/s, given the value of R_e in Table I.

Lastly, if we assume $\overline{Ca}_c \simeq 4$ mM, $\bar{g}_{si} \simeq 25 \times 10^{-6}$ s/cm^2, and $S_m/V_c = (S_m/V_T)/(V_c/V_T) \simeq 1.6 \times 10^6$ cm^{-1}, then from Eq. A20 we find $\tau_c \simeq 1.6$ s and from Eq. A19 we calculate the DC value of $\gamma_c \simeq 3{,}500$ cm^{-1}. Thus, $\gamma_c a$ is indeed large so that extracellular diffusion is slow, but the value of τ_c is also quite slow. In fact, τ_c is about two orders of magnitude too slow to account for inactivation of the slow inward current.

In regard to intracellular accumulation/depletion of Ca^{++}, we can estimate a lower bound on τ_i by assuming $\kappa = 1$ (i.e., intracellular calcium buffering does not exist) and estimating $\overline{Ca}_i \simeq 10^{-7}$M. From Eq. A15 we calculate $\tau_i \geq 0.008$ s, where we assume $S_m/V_i \simeq S_m/V_T$ and other parameter values are in accordance with the above discussion. In Table II, in the voltage range -40 to -20 mV, the value of $1/\omega_2 = 0.017$ s. Thus, if intracellular Ca^{++} buffering is not too effective in this preparation, then intracellular accumulation/depletion of Ca^{++} has the right time constant to explain our data. Because we are using tissue cultured cells, with an immature contractile apparatus and perhaps other deficiencies, it seems possible that κ is on the order of 0.5, so we do not rule out intracellular Ca^{++} changes.

Another explanation of our results is that inactivation is due to a local effect of calcium near the channel mouth, where calcium may bind to a regulatory site which signals the channel to inactivate. Such a mechanism has been suggested for several tissues: aplysia neurons (Tillotson, 1979); insect muscle (Ashcroft and Stanfield, 1981); paramecium (Brehm and Eckert, 1979); and heart muscle (Mentrard et al., 1984).

If we were to perform a linearized analysis of binding to a regulatory site, the amount of calcium bound would almost certainly be proportional to the free calcium concentration. We presume that such a binding site would be on the intracellular side of the channel since our calculation of the time constant for cleft accumulation/depletion is much too slow to explain our data. Accordingly, inactivation of the slow inward current would be proportional to intracellular calcium. In the analysis presented in the Appendix to this paper, we assume that free calcium is proportional to the amount entering the cell, but the proportionality constant, κ, must be less than unity since we know that intracellular calcium is buffered. If, instead, the proportionality constant were to represent the combined effects of intracellular buffering and local binding, then it would not be constrained to be less than unity. Of course, an appropriate model might involve other factors, such as the time constant for the channel to gate subsequent to calcium binding, but to the accuracy of the data presently available, the analysis in the Appendix is probably an adequate linear model of the effect of intracellular accumulation/depletion on either the driving force for current flow or on the modulation of current flow by an intracellular binding site.

Gated Inactivation vs. Intracellular Accumulation

The Appendix shows that accumulation/depletion and gated inactivation of an inward current have fundamentally different effects on the small signal impedance. This interesting result can be better understood if we consider the following simplified situation. Assume that at $t = t_0$ in Fig. 7 *A* we apply a transmembrane voltage-clamp depolarization into a potential range where: (*a*) the activation process of the slow inward current is complete; (*b*) inactivation is incomplete; (*c*) we are significantly negative to the reversal potential. If we have gated inactivation of the channels, any further depolarization (at $t = t_1$ in Fig. 7 *A*) will cause an increase in inactivation. Conversely, if significant intracellular accumulation of calcium has occurred, then further depolarization will reduce the accumulation, or, in effect, reduce the inactivation. This difference is clearly illustrated by considering the current flows sketched in Fig. 7 *B* and *C*, following the step at $t = t_1$.

Regardless of the mechanism of inactivation, a small step depolarization, δv_m, towards E_{Ca} will cause an initial step decrease in inward current through the fraction of the conductance that is not inactivated. In Fig. 7 *C* we have assumed there is no gated inactivation, only apparent inactivation due to Ca accumulation, hence the step in current at $t = t_1$ is greater in Fig. 7 *C* than *B*. If we have gated inactivation, then following the small depolarization δv_m there will be a time-dependent reduction in the conductance as more channels inactivate, consequently we see the time dependent decrease in inward current shown in Fig. 7 *B* (or we record a positive weighting on the frequency

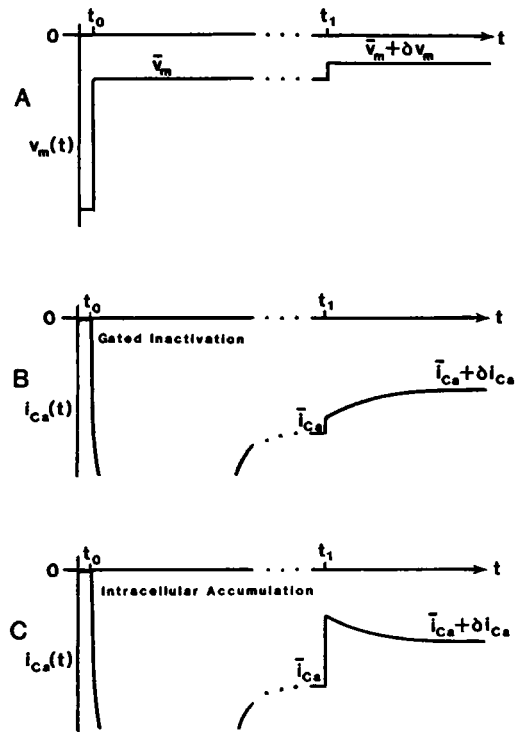

FIGURE 7 An idealized voltage-clamp experiment that illustrates the predicted current flow through the slow inward channel assuming inactivation due to channel gating (*B*), or apparent inactivation due to intracellular calcium accumulation (*C*). (*A*) A voltage clamp pattern that is assumed to step into a potential range, $\bar{v}_m$, which results in total activation of all slow inward channels but incomplete inactivation, as illustrated by the large current, which goes off scale in either *B* or *C* but returns to the steady state value $\bar{i}_{Ca}$. The further depolarization, δv_m, therefore illustrates the inactivation process separately from activation. (*B*) The expected pattern of current flow through the slow inward channels when there is only gated inactivation. Following the application of the step δv_m, there is a time-dependent gated inactivation of the channel causing the illustrated decrease in inward current (note, background currents and the capacity transient are omitted from this idealized sketch). (*C*) The expected pattern of current flow through the slow inward channels when there is no gated inactivation, but calcium has accumulated intracellularly in the time interval $t_0 \le t \le t_1$. At times, $t \ge t_1$, the further depolarization, δv_m, moves the membrane voltage closer to E_{Ca} and therefore causes a reduction in intracellular Ca accumulation. See the text for further discussion.

domain relaxation). However, the small depolarization δv_m also moves the membrane voltage closer to E_{Ca}, so if significant intracellular accumulation of calcium occurred in response to the initial step $\bar{v}_m$, then for $t \ge t_1$ there will be a small time-dependent decrease in intracellular accumulation, which causes the small time-dependent increase in the inward current we see in Fig. 7 *C* (or we record a negative weighting on the frequency domain relaxation).[1]

[1]If it is binding of Ca to an intracellular regulatory site that modulates inactivation, then as the intracellular accumulation is reduced there will be removal of inactivation and an increase in inward current similar to that shown in Fig. 7 *C*. However, Fig. 7 *C* was drawn to illustrate apparent inactivation due to changes in the driving force for Ca current so the initial jump at $t = t_1$ would not necessarily be the same.

The idealized situation just described can probably never be achieved in a real experiment. It was contrived only to help us understand the physical processes that give rise to such a striking difference in the predictions of the models derived in the Appendix, yet it also serves to demonstrate the unique and essential correspondence of frequency domain and time domain analysis. With either technique, given sufficient resolution one would come to the same conclusions. But in the real world of time domain measurements, where we have background currents, capacity transients, spatial/temporal inhomogeneities in membrane voltage and activation overlapping with inactivation, it is unlikely that one could resolve the different transients illustrated in Fig. 7 *B* or *C*. Whereas the sensitivity of the frequency domain techniques described in this paper is sufficient to easily detect the sign of the weighting function for each exponential.

CONCLUSIONS

We report that the small signal impedance technique can be used to study the properties of nonlinear, time and voltage-dependent channels in cardiac muscle. We see two main advantages of the impedance technique. (*a*) It can be used to study properties of channels under conditions in which fast control of transmembrane potential is not possible. (*b*) It is a useful technique in integrating ultrastructural and physiological findings. Many electrophysiologists have moved away from studying tissues with complex geometries because voltage-clamp data in such tissues are difficult to interpret. Nevertheless, these geometric complexities must play an important role in the electrical behavior of the tissue and impedance analysis is a useful tool that helps us to understand the role of structural complexity.

Our results show that the slow inward current in these clusters activates very rapidly and then inactivates with a rather rapid time course. The rapid activation time is similar to that reported by Lee and Tsien (1982) or Matteson and Armstrong (1984) for calcium channels in single cells. Thus, the activation of the calcium channel in syncytial cardiac preparations is probably equally rapid and is an intrinsic property of the channel. The relatively slow activation of the calcium current reported for most cardiac tissue (reviewed in Reuter, 1979) is likely to be due to poor control of membrane potential at short times as suggested by Isengerg and Klöckner (1982). Indeed, the historical reason for studying tissue cultured clusters of chick heart cells was their favorable geometry for fast voltage-clamp studies (Ebihara et al., 1980; Mathias et al., 1981*b*). Despite their apparent utility in studying membrane channels, the rapid inactivation of the slow inward current in this preparation may to be due to the small cell size causing intracellular calcium accumulation, rather than being an intrinsic channel property. Whether this mechanism of inactivation is physiologically relevant in adult heart muscle is not known. However, given the

possibility that geometry may play an important role in the Ca current recorded during voltage clamp of this preparation, one should look to adult heart cells (rather than embryonic heart cells) to study these currents.

APPENDIX

Linear Models of Gating and Accumulation/Depletion

The G_ks and ω_ks in Eq. 1 arise from several processes, so we would like to understand the relationship of these parameters with the physical properties of the clusters. The slow inward current (see the review by Tsien, 1983) serves as a good example. The processes that we will consider are: (*a*) a voltage-dependent activation gate in the slow inward channel; (*b*) a voltage-dependent inactivation gate in the slow inward channel; (*c*) intracellular accumulation/depletion of calcium; and (*d*) intercellular accumulation/depletion of calcium.

Activation Gating. We will assume that current through the slow inward channel is carried primarily by Ca^{++} ions. The channel turns on with depolarization due to a voltage-dependent activation gate, thus if we hold the membrane potential at the depolarized DC voltage, $\bar{v}_m$, and apply small perturbations, δv_m, on top of the DC voltage, the activation gate will be perturbed by δv_m such that a small depolarization will open a few more gates and cause inward current to flow down the electrochemical gradient $\bar{v}_m - E_{Ca}$. The linearized model of such a process has been described (e.g., Hodgkin and Huxley, 1952; Chandler et al., 1962; Mathias et al., 1981) and the frequency domain relationship between current voltage is

$$\delta i_a(j\omega) = \delta v_m(j\omega)\left[\frac{G_a}{1 + j\omega/\omega_a} + \bar{g}_{si}\right], \tag{A1}$$

where ω_a is the sum of the forward and reverse rate constants for activation and the weighting conductance, G_a, is given by

$$G_a = \frac{\partial p_a(\bar{v}_m)}{\partial V_m}(\bar{v}_m - E_{Ca})\bar{g}_{si}. \tag{A2}$$

$\bar{g}_{si}$ is the average conductance of all the slow inward channels at the voltage $\bar{v}_m$ and $p_a(\bar{v}_m)$ is the probability of a channel activating at the voltage, $\bar{v}_m$. Because we are modeling an activation process, the probability of a channel opening increases with depolarization, thus the value of

$$\frac{\partial p_a(\bar{v}_m)}{\partial V_m} > 0. \tag{A3}$$

However, this is an inward current over the range of $\bar{v}_m$ where the channel activates, hence

$$\bar{v}_m - E_{Ca} < 0. \tag{A4}$$

These two observations require that G_a is a negative conductance. Moreover, in the time domain we find that activation of the slow inward channel in these clusters occurs in 1–2 ms, accordingly $\omega_a/2\pi$ is on the order of 150 Hz. At frequencies ~150 Hz the impedance of a cluster has fallen to a value that is just a few percentage of the DC resistance, thus it will be difficult to resolve the activation of the slow inward current in impedance studies. The general properties expected for the activation of the slow inward current are: (*a*) Its natural frequency is rather high and over the range 0.1 to 100 Hz, the average channel's activation gate can accurately follow perturbations in voltage. Thus the gated process produces a current that is in phase with voltage and in this frequency range activation resembles a simple conductance. (*b*) The value of G_a is negative, thus the over the frequency 0.1 to 100 Hz the gated process resembles a negative conductance.

Inactivation Gating. Next consider inactivation of the slow inward current. The inactivation process is much slower and should therefore be easily resolved in our impedance studies. If inactivation is due to a voltage-dependent gate, then the frequency domain representation of the process is

$$\delta i_i(j\omega) = \delta v_m(j\omega)\frac{G_i}{1 + j\omega/\omega_i}, \tag{A5}$$

where ω_i and G_i are defined analogously to ω_a and G_a. Because we are dealing with inactivation, as the membrane becomes more depolarized, the probability of a channel being open is decreasing, hence

$$\frac{\partial p_i(\bar{v}_m)}{\partial V_m} \leq 0. \tag{A6}$$

Accordingly, the weighting conductance, G_i, must be a positive number. The physical properties expected from gated inactivation of the slow inward current are: (*a*) over the frequency range 0.1 to 100 Hz the gating will lag behind voltage changes, hence the process will resemble a combination of conductors and inductors; (*b*) the weighting conductance of inactivation will have the opposite sign from that of activation, the sign of G_i being positive.

Intracellular Accumulation/Depletion. There are other mechanisms that might be responsible for the decline of the slow inward current. The cells comprising a cluster are small and have a large surface-to-volume ratio, thus it is possible for the inward flow of Ca^{++} following activation to cause a significant increase in intracellular Ca^{++} concentration. This would tend to modify E_{Ca} in the direction to shut off membrane current flow. However, there are intracellular buffers for Ca^{++} and we do not know their efficiency.

The total increase in intracellular Ca^{++} is determined by integrating the inward membrane current over time, but the buffers will tend to reduce the free calcium. We can make a first-order correction by including a scale factor κ, which reduces the rate of intracellular accumulation, given a rate of transmembrane influx. Accordingly,

$$\kappa \leq 1, \tag{A7}$$

and the rate of intracellular Ca^{++} accumulation/depletion is approximately given by

$$\frac{4}{3}\pi a^3 \frac{V_i}{V_T}\frac{dCa_i}{dt} = -\frac{\kappa}{FZ}\frac{S_m}{V_T}\frac{4}{3}\pi a^3[g_{si}(V_m - E_{Ca}) + i_p], \tag{A8}$$

where i_p is the rate of active transmembrane transport of Ca^{++}, V_i/V_T is the fraction of intracellular volume per unit volume of tissue, and we have neglected local variations in concentration within a cell (Fischmeister and Horackova, 1983). The total calcium current crossing all the inner membranes is

$$I_{Ca} = \frac{4}{3}\pi a^3 \frac{S_m}{V_T}\{g_{si}(V_m - E_{Ca}) + i_p\}. \tag{A9}$$

These two equations can be linearized by expanding the variables as small perturbations δ about a steady, DC value

$$\begin{aligned} Ca_i &= \overline{Ca_i} + \delta Ca_i; \\ g_{si} &= \bar{g}_{si} + \delta g_{si}; \\ V_m &= \bar{v}_m + \delta v; \\ I_{Ca} &= \bar{i}_{Ca} + \delta i_{Ca}; \\ E_{Ca} &= \bar{E}_{Ca} + \delta E_{Ca}. \end{aligned} \tag{A10}$$

We assume that at steady state, $\bar{v}_m$ is approximately spatially uniform

$$\bar{g}_{si}(\bar{v}_m - \bar{E}_{Ca}) + i_p = 0. \tag{A11}$$

If we neglect terms proportional to δ^2 the linearized version of Eq. A8 is

$$\frac{V_i}{V_T}\frac{d\delta Ca_i}{dt} = -\frac{\kappa}{FZ}\frac{S_m}{V_T}\{\delta g_{si}(\bar{v}_m - \bar{E}_{Ca}) + \delta v_m \bar{g}_{si} - \bar{g}_{si}\delta E_{Ca}\}, \quad (A12)$$

where we can expand the logarithm (Nernst potential) for small perturbations in intracellular calcium as follows:

$$\delta E_{Ca} = -\frac{RT}{FZ}\frac{\delta Ca_i}{\overline{Ca}_i}. \quad (A13)$$

Eq. A12 is therefore linear and we can take its Fourier transform. The first two terms on the right-hand side of Eq. A12 represent the activation process described by Eq. A1, thus their Fourier transform is:

$$\int_{-\infty}^{\infty} e^{-j\omega t}\{\delta g_{si}(\bar{v}_m - \bar{E}_{Ca}) + \delta v_m \bar{g}_{si}\}dt = \delta v_m(j\omega)\left[\frac{G_a}{1 + j\omega/\omega_a} + \bar{g}_{si}\right],$$

but in accordance with the previous discussion, ω_a is sufficiently large that in the frequency range where inactivation is taking place, we can approximate

$$G_{si} \triangleq \bar{g}_{si} + \frac{G_a}{1 + j\omega/\omega_a} \approx \bar{g}_{si} + G_a$$

for small ω. If we linearize the current Eq. A9 and take its Fourier transform, then substituting the transform of Eq. A12 yields

$$\delta i_{Ca}(j\omega) = \frac{4}{3}\pi a^3 \frac{S_m}{V_T}\left[G_{si} - \frac{G_{si}}{1 + j\omega v_i}\right]\delta v_m(j\omega), \quad (A14)$$

where the time constant of intracellular accumulation/depletion is given by

$$\tau_i = \frac{(FZ)^2\overline{Ca}_i}{\kappa RT\bar{g}_{si}S_m/V_i}. \quad (A15)$$

At most voltages G_{si} will be a positive number since G_a goes to zero as all of the channels become activated (i.e., $\partial p_a[\bar{v}_m]/\partial V_m \to 0$ as $p_a[\bar{v}_m] \to 1$). This implies the weighting conductance of an inactivation process due to intracellular accumulation/depletion will, at most voltages, be a negative number whereas a gated inactivation must always be a positive number. Hence, there is an unequivocal distinction between these two mechanisms when one studies their small signal, linear behavior, whereas their large signal, nonlinear behavior cannot be distinguished without ion substitutions or other manipulations.

Intercellular Accumulation/Depletion. The last mechanism we would like to consider is inactivation due to depletion of Ca^{++} from the small intercellular clefts. This is somewhat more complicated than the intracellular problem, owing to the conduction and diffusion of Ca^{++} from the bath into the intercellular spaces. However, Ca^{++} is a small fraction of the total ions in the bath and radial voltage gradients along the intercellular spaces are small, thus it can be shown that conduction of Ca^{++} is small compared to diffusion. The rate of extracellular change is therefore well approximated by

$$\frac{V_c}{V_T}\frac{\partial Ca_c}{\partial t} = \frac{1}{2F}\frac{S_m}{V_T}\{g_{si}[V_m = E_{ca}] + i_p\} + D_c\frac{1}{r^2}\frac{\partial}{\partial r}\left(r^2\frac{\partial Ca_c}{\partial r}\right), \quad (A16)$$

where D_c is the effective diffusion coefficient for the intercellular clefts and Ca_c is the cleft concentration of calcium. We can once again expand all parameters as small deviations about their mean values, and we assume approximate steady state conditions at the DC voltage $\bar{v}_m$. Namely,

$$0 = \frac{1}{2F}\frac{S_m}{V_T}\{\bar{g}_{si}[\bar{v}_m - \bar{E}_{ca}] + i_p\} + D_c\frac{1}{r^2}\frac{d}{dr}\left(r^2\frac{d\overline{Ca}_c}{dr}\right). \quad (A17)$$

The Fourier transform of the linearized version of Eq. A16 is:

$$\frac{1}{r^2}\frac{d}{dr}\left(r^2\frac{d\delta Ca_c}{dr}\right) - \gamma_c^2\delta Ca_c = -\frac{1}{2FD_c}\frac{S_m}{V_c}G_{si}\delta v_m(j\omega), \quad (A18)$$

where

$$\gamma_c^2 = \frac{1}{D_c v_c}(1 + j\omega\tau_c); \quad (A19)$$

$$\tau_c = \frac{(2F)^2\overline{Ca}_c}{RT\bar{g}_{si}S_m/V_c}. \quad (A20)$$

The solution of Eq. A18 can be written as

$$\delta Ca_c = \frac{FZ\,\overline{Ca}_c}{RT\bar{g}_{si}}\frac{G_{Ca}\delta v_m(j\omega)}{1 + j\omega\tau_c}\left(1 - \frac{a\sinh\gamma_c r}{r\sinh\gamma_c a}\right). \quad (A21)$$

If we next linearize Eq. A9, then substitute Eq. A21 into the result, we obtain an equation for current flow. We have shown radial gradients in voltage are small, but Eq. A21 shows there will be a radial variation in the chemical potential of calcium. To compute the total current at the outer surface, crossing the inner membranes, we integrate the membrane current over the volume of tissue to obtain

$$\delta i_{Ca} = \frac{4}{3}\pi a^3\frac{S_m}{V_T}\delta v_m(j\omega)\left\{G_{si} - \frac{G_{si}}{1 + j\omega v_c}[1 - D_{Ca}(j\omega)]\right\}, \quad (A22)$$

where

$$D_{Ca}(j\omega) = \frac{3}{\gamma_c a}\left(\coth\gamma_c a - \frac{1}{\gamma_c a}\right). \quad (A23)$$

Note that

$$\lim_{\gamma_c a \to 0} D_{Ca} = 1.$$

This implies that if diffusion is sufficiently rapid, there will be no intercellular concentration changes. However, if one substitutes typical parameter values (see Results), diffusion is indeed rather slow, hence $\gamma_c a$ is in general a large parameter, and in this limit

$$D_{Ca} \approx \frac{3}{\gamma_c a}, |\gamma_c a| \gg 1.$$

In the Theory section, we presented the model used to fit our data (Eqs. 1 and 2) and those equations are not as complicated as the above analysis. Nevertheless, if diffusion is slow and can be neglected, the effect of extracellular accumulation/depletion can be modeled as a negative weighting conductance and a first-order frequency response, just as the model in Eq. 1. Thus, either extracellular or intracellular accumulation/depletion will usually appear as a negative term in Eq. 6, whereas gated inactivation of the slow inward channel will always appear as a positive term.

We gratefully acknowledge the excellent technical assistance of Ms. Phyllis Bullock who tissue cultured the heart cells. We also are grateful for the support of Dr. R. S. Eisenberg.

This work was supported by the National Institute of Health grant HL 29205, HL 20230, and American Heart Association grant 79-851, with funds in part from the Chicago Heart Association.

Received for publication 13 December 1984 and in final form 29 April 1985.

REFERENCES

Almers, W., and P. T. Palade. 1981. Slow calcium and potassium currents across frog muscle membranes: measurements with a Vaseline-gap technique. *J. Physiol. (Lond.).* 312:159–176.

Almers, W., R. Fink, and P. T. Palade. 1981. Calcium depletion in frog muscle tubules: the decline of calcium under maintained depolarization. *J. Physiol. (Lond.).* 312:177–207.

Ashcroft, F. M., and P. R. Stanfield. 1981. Calcium dependence of the inactivation of calcium currents in skeletal muscle fibers of an insect. *Science (Wash. DC).* 213:224–226.

Attwell, D., D. Eisner, and I. Cohen. 1979. Voltage clamp and tracer flux data: effects of restricted extracellular space. *Q. Rev. Biophys.* 12:213–261.

Bodewei, R., S. Hering, B. Lanke, L. V. Rosenshtraukh, A. I. Undrovinas, and A. Wollengerg. 1982. Characterization of the fast sodium current in isolated rat myocardial cells. *J. Physiol. (Lond.).* 325:301–315.

Brehm, P., and R. Eckert. 1979. Calcium entry leads to inactivation of calcium channel in Paramecium. *Science (Wash. DC).* 202:1203–6.

Brown, A. M., K. S. Lee, and T. Powell. 1981. Sodium current in single rat heart muscle cells. *J. Physiol. (Lond.).* 318:455–477.

Cachelin, A. B., J. E. DePeyer, S. Kokubum, and H. Reuter. 1983. Sodium channels in cultured cardiac cells. *J. Physiol. (Lond.).* 340:389–401.

Chandler, W. K., R. FitzHugh, and K. S. Cole. 1962. Theoretical stability properties of a space-clamped axon. *Biophys. J.* 2:105–127.

Clapham, D. E., and L. J. DeFelice. 1982. Small impedance of heart cell membranes. *J. Membr. Biol.* 67:63–71.

Clay, J. R., and A. Shrier. 1981*a*. Analysis of subthreshold pace-maker current in chick embryonic heart cells. *J. Physiol. (Lond.).* 312:471–490.

Clay, J. R., and A. Shrier. 1981*b*. Developmental changes in subthreshold pacemaker currents in chick embryonic heart cells. *J. Physiol. (Lond.).* 312:491–504.

DiFrancesco, D. 1981. A new interpretation of the pacemaker current in calf Purkinje fibers. *J. Physiol. (Lond.).* 314:359–376.

Ebihara, L., N. Shigeto, M. Lieberman, and E. A. Johnson. 1980. The initial inward current in spherical clusters of embryonic chick hearts. *J. Gen. Physiol.* 75:437–456.

Eisenberg, R. S., V. Barcilon, and R. T. Mathias. 1979. Electrical properties of spherical syncytia. *Biophys. J.* 25:151–180.

Fischmeister, R., and M. Horackova. 1982. Variation of intracellular Ca^{2+} following Ca^{2+} current in heart. A theoretical study of ionic diffusion inside a cylindrical cell. *Biophys. J.* 41:341–348.

Fishman, H. M., D. Poussart, and L. E. Moore. 1979. Complex admittance of Na^+ conduction in squid axon. *J. Membr. Biol.* 50:43–63.

Fishman, H. M., L. E. Moore, and D. Poussart. 1981. Squid axon K conduction: admittance and noise during short- versus long-duration step clamps. *In* The Biophysical Approach to Excitable Systems. W. J. Adelman, Jr., editor. Plenum Publishing Corp., New York. 65–94.

Fitzhugh, R. 1960. Thresholds and plateaus in the Hodgkin-Huxley nerve equations. *J. Gen. Physiol.* 43:867–896.

Hodgkin, A. L., and A. F. Huxley. 1952. A quantitative description of membrane current, and its application to conduction, and excitation in nerve. *J. Physiol. (Lond.).* 117:500–544.

Hume, J. R., and W. Giles. 1983. Ionic currents in single isolated bullfrog atrial cells. *J. Gen. Physiol.* 81:(2)153–94.

Isenberg, G., and U. Klöckner. 1982. Calcium currents of isolated bovine ventricular myocytes are fast and of large amplitude. *Pfluegers Arch. Eur. J. Physiol.* 395:30–41.

Josephson, J., and N. Sperelakis. 1982. On the ionic mechanism underlying adrenergic cholinergic antagonism in ventricular muscle. *J. Gen. Physiol.* 79:69–86.

Kaign, M. E., J. D. Ebert, and P. M. Stott. 1966. The susceptibility of differentiating muscle clones to Ronus sarcoma virus. *Proc. Natl. Acad. Sci. USA* 56:133–140.

Kass, R. S. 1984. Delayed rectification in the cardiac Purkinje fiber is not activated by intracellular calcium. *Biophys. J.* 45:837–839.

Lee, K. S., T. A. Weeks, R. L. Kao, N. Akaike, and A. M. Brown. 1979. Sodium current in single heart muscle cells. *Nature (Lond.).* 278:269–271.

Lee, K. S., and R. W. Tsien. 1982. Reversal of current through calcium channels in dialysed single heart cells. *Nature (Lond.).* 297:498–501.

Levis, R. A., R. T. Mathias, and R. S. Eisenberg. 1983. Electrical properties of sheep Purkinje strands. Electrical and chemical potentials in the clefts. *Biophys. J.* 44:225–248.

Lux, H. D., E. Neher, and A. Marty. 1981. Single channel activity associated with calcium dependent outward current in Helix pomatia. *Pfluegers Arch. Eur. J. Physiol.* 389:293–295.

Marty, A. 1981. Ca-dependent K channels with large unitary conductance in chromaffin cell membranes. *Nature (Lond.).* 291:497–500.

Mathias, R. T. 1983. Effect of tortuous extracellular pathways on resistance measurements. *Biophys. J.* 42:55–59.

Mathias, R. T., J. L. Rae, and R. S. Eisenberg. 1979. Electrical properties of structural components of the crystalline lens. *Biophys. J.* 25:181–201.

Mathias, R. T., J. L. Rae, and R. S. Eisenberg. 1981*a*. The lens as a nonuniform spherical syncytium. *Biophys. J.* 34:61–83.

Mathias, R. T., L. Ebihara, M. Lieberman, and E. A. Johnson. 1981*b*. Linear electrical properties of passive and active currents in spherical heart cell clusters. *Biophys. J.* 36:221–242.

Matteson, D. R. and C. M. Armstrong. 1984. Na and Ca channels in a transformed line of anterior pituitory cells. *J. Gen. Physiol.* 83:371–394.

Meech, R. W. 1978. Calcium-dependent potassium activation in nervous tissues. *Annu. Rev. Biophys. Bioeng.* 7:1–18.

Mentrard, D., G. Vassort, and R. Fischmeister. 1984. Calcium-mediated inactivation of the calcium conductance in cesium-loaded frog heart cells. *J. Gen. Physiol.* 83:105–131.

Nathan, R. D., and R. L. DeHaan. 1979. Voltage clamp analysis of embryonic heart cell aggregates. *J. Gen. Physiol.* 73:175–198.

Reuter, H. 1979. Properties of two inward membrane currents in the heart. *Annu. Rev. Physiol.* 41:413–424.

Reuter, H., C. F. Stevens, R. W. Tsein, and G. Yellen. 1982. Properties of single calcium channels in cardiac cell culture. *Nature (Lond.).* 297:501–504.

Tillotson, D. 1979. Inactivation of Ca conductance dependent on entry of Ca ions in molluscan neurons. *Proc. Natl. Acad. Sci. USA.* 76:1497–1500.

Tsien, R. W. 1983. Calcium channels in excitable cell membranes. *Annu. Rev. Physiol.* 45:341–358.